
COCOTREE: A Dataset and Benchmark for Open Tree-Structured Visual Decomposition

Junhyub Lee
Chung-Ang University
junhyub3090@cau.ac.kr

Seunghun Chae
Chung-Ang University
ch040602@cau.ac.kr

Hyosu Kim
Chung-Ang University
hskimhello@cau.ac.kr

Abstract

We formalize and enable the task of *open tree decomposition*, which segments an image into hierarchical trees of visual components with unconstrained granularity and flexibility. Specifically, we provide the foundation benchmark for this new paradigm with the following three key contributions. First, we overcome the prohibitively high cognitive and physical bottlenecks of manual annotation by developing a fully automated generation pipeline that synergizes the semantic reasoning of Large Vision-Language Models (LVLMs) with the precise geometric grounding of SAM 3. Second, leveraging this pipeline, we construct COCOTREE, a massive-scale benchmark featuring over 21K images and 1.8M structural nodes. By embracing an open-vocabulary space of over 3.5K unique labels, it successfully captures the long-tail distribution of complex physical assemblies. Notably, rigorous human evaluation confirms our generated annotations demonstrate strong alignment with human structural judgment. Third, we establish a standardized evaluation protocol by proposing the Open Tree Quality (OTQ) metric, which jointly assesses mask precision, label accuracy, and structural consistency. We release our dataset and benchmark code at <https://github.com/melonkick3090/COCOTree>.

1 Introduction

Image segmentation has long served as a fundamental pillar of visual recognition. It partitions an image into either semantic category regions, distinct object instances, or panoptic outputs at the pixel level [19, 10, 11]. In particular, recent advances in image segmentation have enabled the segmentation of images into extremely fine-grained units, e.g., constituent parts of objects [24], providing granular comprehension of complex physical environments.

However, existing methods typically provide a single-level abstraction of these fine-grained components, entirely ignoring the hierarchical dependencies inherent in real-world assemblies. This lack of structural information not only hinders compositional reasoning over visual scenes but also causes severe functional ambiguity: an isolated "handle" segment provides no structural clues as to whether it can be used to open a door, hold a cup, or turn a mechanical valve. These problems pose a critical bottleneck for autonomous systems, such as embodied AI agents, which require complex physical manipulation rather than mere visual perception.

In response to the need for hierarchical image understanding, hierarchical datasets [3, 5, 9, 26, 16] have been introduced. These datasets capture compositional relationships but with severe limitations in granularity and flexibility. First, they primarily confine their structural depth to single-step object-part dependencies, rarely extending to the deeper sub-part hierarchies. This shallow abstraction thus loses the deep, critical structural chain of objects (e.g., tracing from a car, to its door, but not down to the specific door handle). Furthermore, these structural annotations are strictly constrained by closed-set vocabularies. Such a rigid taxonomy-based annotation might be effective for object recognition, but is entirely inadequate for modeling the unconstrained compositional structures

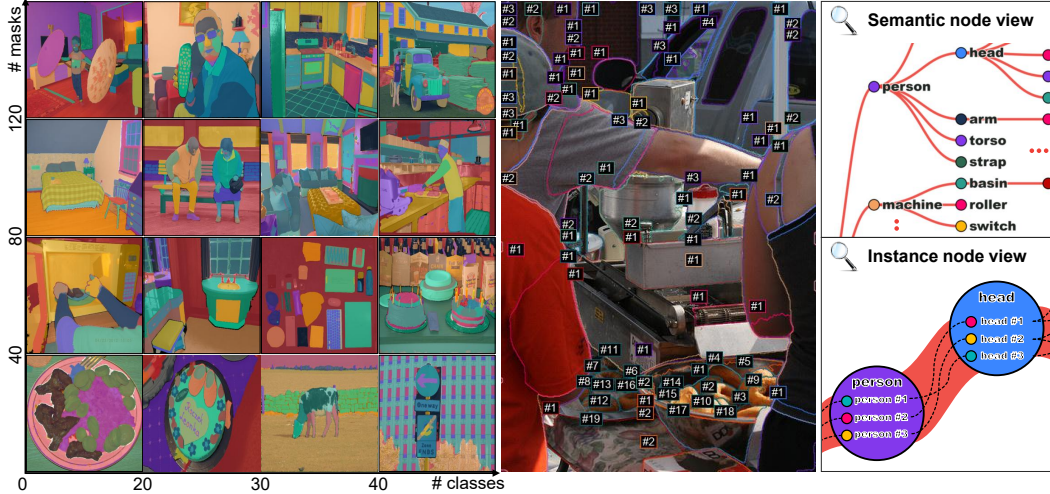


Figure 1: Overview of COCOTREE. Left: COCOTREE provides dense open-tree annotations over COCO images. Middle: each image is decomposed into visible components grounded by instance masks. Right: the same annotation can be viewed as a semantic-node tree, which groups repeated masks under a shared local label, and as an instance-node tree, where each mask becomes a node with an explicit visual parent.

inherent to the real world. That is, these datasets ignore any novel, long-tail components or structural configurations falling outside the taxonomies, although they are clearly present in the images.

In this paper, we facilitate the development of algorithms for hierarchical analysis with unconstrained granularity and flexibility, a task which we call *open tree decomposition*. Specifically, we provide a large-scale dataset in which images are represented as hierarchical trees of visible components, called *open trees*. Each node in the tree encapsulates a single instance mask paired with its corresponding semantic label. In particular, the tree’s hierarchical structure and each node’s label are derived from the unconstrained visual reality of the image, rather than forced into a predefined template.

However, constructing such highly granular annotations through human labor is prohibitively challenging at scale. Even worse, deriving unconstrained structural and linguistic annotations based on the given visual evidence exponentially amplifies the cognitive burden. To overcome the fundamental limitations of manual annotation, we develop a fully automated annotation pipeline that recursively leverages recent Large Vision-Language Models (LVLMs) and SAM 3 [2]. Starting from the entire scene, it prompts LVLMs for a semantic decomposition of the current visual region. These semantic proposals are then spatially grounded into precise instance masks by SAM 3. Each generated mask is subsequently cropped and fed back into the LVLM as a new parent node, repeating this cycle until the model determines no further meaningful subdivisions exist.

Finally, we introduce COCOTREE, built upon this automated pipeline. Originating from the COCO dataset [17], COCOTREE benefits from a high density of complex, interacting objects within everyday environments like other COCO-based datasets [8, 6, 26, 5], while simultaneously providing unprecedented hierarchical granularity and flexibility (see examples in Fig. 1). It features over 21K images and 1.8M total instance masks (i.e., nodes), achieving an incredibly dense annotation rate of 85.7 masks per image and an average tree depth of 3.448. Furthermore, it catalogs over 3.5K unique open-vocabulary labels, successfully capturing the long-tail distribution of real-world physical components. It should be noted that we ensured the practical utility of these automated annotations by assessing their quality via extensive human evaluation, which confirms strong alignment with human judgment regarding both hierarchical structures and open-vocabulary labeling. COCOTREE then serves as a benchmark for open tree decomposition tasks with a metric, called *Open Tree Quality (OTQ)*. This is a PQ (Panoptic Quality [11])-like metric that jointly evaluates mask quality, label quality, and structural consistency.

2 Related Work

2.1 Hierarchical Segmentation

Hierarchical segmentation datasets have extended image segmentation beyond a single level of abstraction by annotating visual structures. Specifically, numerous benchmarks capture the compositional relationships between parent objects and their part components [3, 9, 26, 21]. Recently, this hierarchical granularity has been further increased to capture part-subpart relationships in natural images [36, 24]. Despite these advancements, existing paradigms force visual representations into rigid, predefined templates. By limiting structural hierarchies to a shallow, two- or three-tier depth and restricting labels to a closed vocabulary, these datasets strip away the unconstrained structural context of the physical world. This shallow abstraction creates a fundamental data bottleneck for complex compositional reasoning. In addition, diverse metrics have been introduced as evaluation protocols for hierarchical segmentation. For instance, PartPQ (part panoptic quality) [5] extends standard panoptic quality to assess segmentation performance across a strict two-level object-part hierarchy, while HPQ (hierarchical panoptic quality) [31] broadens this to evaluate fixed, multi-tier semantic hierarchies. Despite their utility, both metrics systematically fail when applied to unconstrained-granularity, open-vocabulary structures.

Consequently, hierarchical segmentation models have traditionally mirrored these structural constraints. While they support the prediction of basic object-part relations [16] or even more granular hierarchies [15, 33, 14, 31], they inherently operate within predefined semantic taxonomies or structural depths.

2.2 Hierarchical Vision-Language Segmentation

With recent advance of LVLMs (Large Vision-Language Models) [18], the paradigm of image segmentation has increasingly shifted towards open-vocabulary, instruction-driven parsing. Recent frameworks seamlessly couple the semantic reasoning of LVLMs with dense segmentation tasks [13, 29, 32, 27]. In particular, GLaMM [27] demonstrates that automated annotation pipelines powered by LVLMs can successfully drive the generation of large-scale segmentation datasets. In addition, the visual reasoning capabilities of LVLMs have been integrated into dense segmentation pipelines [32, 4, 34, 35], typically by prompting geometric foundation models like SAM [12] and SAM 3 [2]. However, these systems inherently treat segmentation as a static, single-level task, resulting in the lack of the structural awareness necessary to parse complex, multi-level compositional assemblies.

To bridge this gap, several recent methods have moved from flat open-vocabulary segmentation toward structured, hierarchical prediction. Language-conditioned segmentors now produce masks at varying semantic levels, leveraging the reasoning capabilities of LVLMs to generate grounded hierarchical outputs [33, 14, 31, 13, 29, 32, 27]. HALLUMI [23] generates hierarchical segmentation masks via autoregressive language modeling to capture object-part-subpart granularity under predefined structural taxonomies.

3 COCOTREE: Task, Construction, and Dataset

For a comprehensive understanding of COCOTREE, a dataset and benchmark for open tree decomposition, we first formulate the open tree decomposition task, detail the automated, recursive annotation pipeline for constructing a large-scale hierarchical dataset, and summarize the scale and structure of the resulting dataset.

3.1 Open Tree Decomposition Task Formulation

Given an input image $I \in \mathbb{R}^{H \times W \times 3}$, traditional hierarchical segmentation tasks typically map pixels to a predefined set of categories C with a strictly bounded hierarchical depth. In contrast, we formulate open tree decomposition as the task of parsing the image I into an unconstrained hierarchical tree, called an *open tree*, directly derived from the visual evidence of I . The open tree is structured as $T = (V, E)$:

- *Nodes (V , visible components)*. Each node $v_i \in V$ represents a distinct visual component in the image I and is defined as a tuple $v_i = (m_i, l_i)$. Here, $m_i \in \{0, 1\}^{H \times W}$ is a binary instance mask

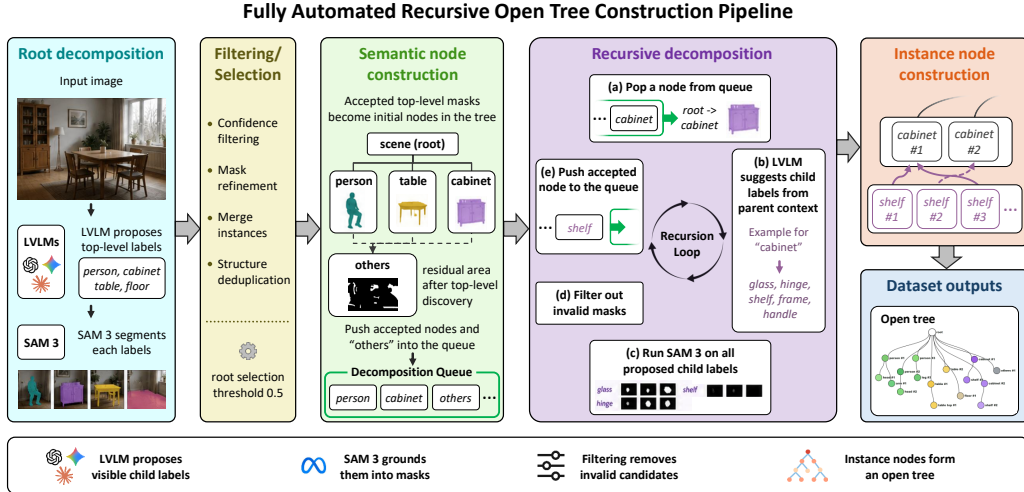


Figure 2: Fully automated open tree construction pipeline.

spatially grounding the component, and $l_i \in \mathcal{L}$ is its corresponding semantic label. Unlike prior work, \mathcal{L} represents an open-vocabulary linguistic space, allowing l_i to capture any long-tail or unconstrained text description.

- *Edges (E , structural hierarchy)*. The edge set E captures the compositional relationships between visible components. A directed edge $e_{i,j} \in E$ (from parent v_i to child v_j) exists if and only if v_j is a constituent sub-part visually encompassed by v_i in the image I .

The fundamental distinction of T is its infinite-depth structural flexibility. The tree originates from a universal root node r (representing the entire scene I) and recursively branches based solely on the physical complexity of the objects present, terminating at leaf nodes where no further meaningful sub-divisions exist.

3.2 Fully Automated Open Tree Annotation Pipeline

Open tree annotation is a recursive generation process that derives labels, masks, and structural relationships directly from visual evidence. However, executing this unconstrained decomposition through manual human annotation presents severe scalability and consistency bottlenecks. We therefore automate open tree annotation with a recursive pipeline that combines the unconstrained semantic reasoning of LVLMs with the highly dense, precise localization of vision foundation models (SAM 3). In particular, to ensure computational scalability, this recursive decomposition is driven at the semantic level rather than the instance level in the following steps (see Figure 2).

Root decomposition. The generation process initializes by deconstructing the highest-level visual context (the root node). First, the LVLm analyzes the unconstrained image to propose common-noun labels for the major constituent elements in the scene. The proposal prompt strictly on visible evidence, filtering out materials, abstract attributes, and near-synonyms to prevent hallucination (see Appendix A). Second, these semantic proposals are passed to the vision foundation model, which grounds them into precise spatial masks, isolating primary objects, distinct scene regions, and broad contextual background elements (i.e., ‘stuff’). A single proposed label may yield multiple grounded masks corresponding to distinct visible instances; these are structurally grouped to form a semantic node. The geometric union of these grouped masks defines the visual context for subsequent recursive decomposition, while the individual instance masks are retained for the final open tree materialization. Finally, these foundational semantic nodes are connected via directed edges to the root node. Note that this initial pipeline also records an *others* region for uncovered pixels used for further decomposition.

Recursive decomposition. Once initialized, all newly generated semantic nodes are enqueued to drive the recursive expansion of the tree. For each node within the queue, the pipeline extracts a

Table 1: Dataset scale and density. M/img denotes masks per image. $MaxD$ denotes maximum hierarchy depth.

Dataset	Images	Masks	M/img	Classes	$MaxD$
COCO-17 [17]	118K	860K	7.3	80	1
COCO-Stuff [1]	118K	1.0M	8.5	91	1
COCONut [6]	358K	4.7M	13.1	133	1
COCO-ReM [30]	118K	1.1M	9.3	80	1
LVIS [8]	100K	1.3M	13.0	1.2K	1
PACO [26]	77K	901K	11.7	531	2
CPP [5]	3.5K	156K	44.6	28	2
PartImageNet [9]	24K	136K	5.7	198	2
SPIN [24]	10K	146K	14.6	254	3
ADE20K [36]	20K	270K	13.5	150	3
COCOTREE	21K	1.8M	85.7	3.5K	Unconstrained

Table 2: Node depth distribution by size bin. Columns sum to 100%.

Depth	All	XS	S^*	M	L
1	27.7	7.0	21.3	36.9	69.8
2	42.3	36.6	45.0	45.9	26.1
3	23.9	39.1	27.6	15.6	3.9
≥ 4	6.1	17.3	6.1	1.6	0.2

strictly isolated visual representation: the original image is tightly cropped to the spatial extents of the node’s grouped mask, and all external background pixels are suppressed. This localized visual crop is then fed back into the LVLMM with its corresponding semantic label and hierarchical structure, re-initiating the semantic proposal phase to uncover sub-components. This iterative loop dynamically expands the tree, treating every extracted part as a new parent until structural exhaustion is reached.

Evidence-based filtering. During the decomposition process, the pipeline retains semantic nodes only if they are supported by sufficient grounding evidence. To achieve this, we employ a scale-adaptive filtering strategy for child mask extraction. Specifically, the confidence threshold of the vision foundation model is dynamically adjusted based on the parent node’s spatial footprint: if the parent mask occupies less than 5% of the full image area, the threshold is relaxed to 0.4 to ensure the successful capture of fine-grained sub-parts; otherwise, a stricter threshold of 0.5 is applied to prevent the extraction of low-confidence noise in larger regions. We also reject semantic nodes whose masks cover more than 70% of the global scene or 90% of their immediate parent mask. For sibling cleanup, we resolve duplicate component proposals by evaluating their geometric intersection. If the spatial overlap between two sibling masks exceeds 90%, they are merged into a single representation to eliminate redundant structural branches.

Instance-level open tree conversion. After recursive semantic decomposition is complete, the intermediate tree of semantic nodes is materialized into an instance-level hierarchy. First, the grouped masks within each semantic node are separated. Each individual mask is instantiated as a distinct node paired with its semantic label. Next, to establish instance-level structural dependencies, lower-level instance masks are assigned to their corresponding parent masks based on spatial containment and overlap heuristics. In cases of ambiguity where a child spatially intersects multiple potential parents, it is deterministically routed to the parent demonstrating the strongest containment evidence. Conversely, child nodes lacking a reliable parent are rejected as noise.

3.3 COCOTREE Analysis

Leveraging the aforementioned automated pipeline across the COCO dataset, we constructed COCOTREE. Before establishing its utility as an evaluation benchmark, we validate COCOTREE as a standalone reference dataset as follows¹.

Scale and structure. As summarized in Table 1, COCOTREE achieves an unprecedented annotation density, averaging 85.7 masks per image. This massive scale dwarfs traditional flat-hierarchy baselines like LVIS (13.0 masks/img) and COCONut (13.1 masks/img), and nearly doubles the density of the most granular hierarchical baseline, CPP (44.6 masks/img). Structurally, while existing hierarchical datasets are bounded to maximum depths of 2 or 3, our automated pipeline expands to an unconstrained depth. Notably, this unconstrained depth perfectly reflects physical object composition.

¹We use four mask-size bins for dataset analysis and flat-mask compatibility: XS : $0 < A < 10^2$, S^* : $10^2 \leq A < 32^2$, M : $32^2 \leq A < 96^2$, and L : $A \geq 96^2$

Table 3: Mask compatibility with existing flat-hierarchy segmentation annotations. Size columns report AR by mask-size bin.

Reference	IoU \uparrow		AR \uparrow						
	Mean	Median	AR	AR@50	AR@75	AR _{XS}	AR _{S+}	AR _M	AR _L
COCO-17	0.69	0.81	0.56	0.80	0.62	0.13	0.45	0.64	0.82
COCONut	0.69	0.83	0.58	0.80	0.64	0.14	0.42	0.69	0.88
COCO-ReM	0.69	0.90	0.63	0.74	0.67	0.15	0.52	0.80	0.90
LVIS	0.54	0.73	0.45	0.60	0.49	0.08	0.40	0.71	0.87

Table 4: Human validation response distributions. Values are percentages with standard deviations.

Q	Axis	Good \uparrow	Minor	Moderate	Major \downarrow	Not clear
<i>Node-level questions</i>						
Q1	Label-mask match	92.9 \pm 2.1	–	–	5.2 \pm 1.5	2.0 \pm 1.7
Q2	Target coverage	71.7 \pm 4.7	18.5 \pm 4.1	–	9.6 \pm 3.6	0.1 \pm 0.1
Q3	Extra instance	88.3 \pm 3.2	9.1 \pm 2.3	–	2.5 \pm 2.0	0.2 \pm 0.2
Q4	Instance separation	91.4 \pm 7.3	5.8 \pm 4.9	2.4 \pm 2.5	0.3 \pm 0.6	0.1 \pm 0.3
Q5	Boundary quality	79.2 \pm 11.3	16.8 \pm 10.2	3.5 \pm 2.2	0.4 \pm 0.7	0.1 \pm 0.2
Q6	Child validity	93.3 \pm 5.9	4.9 \pm 4.7	–	1.3 \pm 1.9	0.5 \pm 1.0
Q7	Child missing	91.8 \pm 9.1	7.3 \pm 8.2	–	0.6 \pm 0.9	0.3 \pm 0.7
Q8	Leaf appropriateness	98.4 \pm 1.5	–	–	1.5 \pm 1.5	0.1 \pm 0.1
<i>Tree-level questions</i>						
T1	Tree consistency	47.5 \pm 23.7	44.3 \pm 19.9	7.1 \pm 6.8	1.0 \pm 2.0	0.1 \pm 0.4
T2	Missing critical nodes	50.5 \pm 16.9	41.6 \pm 13.9	–	7.7 \pm 5.2	0.2 \pm 0.6

While 69.8% of Large (L) masks reside at depth 1 (representing macro-objects), the tree successfully isolates fine-grained sub-parts, with over 56.4% of Extra Small (XS) masks securely grounded at depths of 3 or greater (see Table 2).

Mask compatibility. To verify the geometric quality of our automated annotations, Table 3 evaluates the mask compatibility of COCOTREE against established flat-hierarchy datasets. Overall, our generated masks exhibit high alignment with manual human annotations, achieving a Median IoU of ranging from 0.73 (against LVIS) to 0.90 (against COCO-ReM). In particular, it recovers the vast majority of Large (L) and Medium (M) reference masks (e.g., AR_L of 0.90 against COCO-ReM). However, the recall drops for XS masks. Such tiny regions are difficult for LVLMs to propose from visual evidence and for the visual foundation model to ground reliably, which resulted in performance drops against LVIS, a benchmark uniquely characterized by its significantly higher proportion of long-tail, extra-small masks than standard COCO variants.

Human validation. Our human validation study comprised 20 reviewers who each analyzed 50 randomly-selected images paired with their corresponding open trees. Utilizing a custom web interface, the reviewers qualitatively assessed the accuracy and quality of every semantic node (the interface UI and full questionnaire are detailed in Appendices B and B.1). As reported in Table 4, the generated open trees exhibit high quality at the node level. The automated pipeline excels at node construction, achieving $\geq 91\%$ Good ratings for semantic matching (Q1), instance separation (Q4), child validity (Q6), and leaf appropriateness (Q8). While full-tree consistency (T1) and critical node coverage (T2) exhibit higher rates of Minor issues (44.3% and 41.6%, respectively), an expected outcome given the unconstrained, open-vocabulary nature of the structural generation, Major failures remain critically low (1.0% to 7.7). These results definitively confirm that our fully automated pipeline generates structurally coherent, high-fidelity hierarchical annotations that align closely with human perception.

4 Open Tree Quality and Benchmarking

4.1 Metric Design

COCOTREE requires a metric for image-specific visible trees with open-vocabulary labels. Such outputs are difficult to evaluate because correct masks alone do not guarantee correct open-tree

predictions: a region may be mislabeled, assigned to the wrong parent, duplicated, missed, or stopped at the wrong decomposition level. We introduce Open Tree Quality (OTQ), a PQ-style metric for open tree decomposition. OTQ evaluates this target in three parts. First, predicted and reference nodes are globally matched by mask IoU. Second, each true-positive node is scored by mask IoU and open-label similarity. Third, matched nodes are checked for structural consistency through their visual parents, and unmatched masks are penalized with a PQ-style denominator. The final score combines branch quality with the mean quality of matched mask-nodes.

4.2 Node Matching and Matched-Node Quality

Let $G = (V, E)$ be the reference tree and $P = (\hat{V}, \hat{E})$ be the predicted tree. Each reference node $v \in V$ has an instance mask m_v , a local label ℓ_v , and a parent $\text{pa}(v)$. Each predicted node $\hat{v} \in \hat{V}$ similarly has $\hat{M}_{\hat{v}}$, $\hat{\ell}_{\hat{v}}$, and $\text{pa}(\hat{v})$.

A one-to-one node assignment \mathcal{A} between predicted and reference nodes is obtained by maximum-weight bipartite matching over $\text{IoU}(\hat{v}, v)$.

A matched pair is accepted as a TP_{node} when its IoU exceeds the node threshold $\tau_{\text{node}} = 0.5$:

$$TP_{\text{node}} = \{(\hat{v}, v) \in \mathcal{A} \mid \text{IoU}(\hat{v}, v) \geq \tau_{\text{node}}\}. \quad (1)$$

All predicted nodes not included in TP_{node} are FP_{node} , and all reference nodes not included in TP_{node} are FN_{node} .

For each true-positive node match (\hat{v}, v) , mask quality(MQ) and label quality(LQ) are defined as follows:

$$MQ(\hat{v}, v) = \text{IoU}(\hat{v}, v), \quad LQ_m(\hat{v}, v) = \text{Sim}_m(\hat{\ell}_{\hat{v}}, \ell_v), \quad (2)$$

where m denotes the label-similarity protocol, including strict matching, WordNet/OEWN-based similarity [22, 20], BERT/SBERT-based similarity [7, 28], or another released backend such as CLIP [25].

The matched-node quality and the mean quality over matched nodes are:

$$NQ_m(\hat{v}, v) = MQ(\hat{v}, v) \cdot LQ_m(\hat{v}, v), \quad \text{meanNQ}_m = \frac{1}{|TP_{\text{node}}|} \sum_{(\hat{v}, v) \in TP_{\text{node}}} NQ_m(\hat{v}, v). \quad (3)$$

If there are no true-positive node matches, we set $\text{meanNQ}_m = 0$, and the final OTQ score is zero.

For diagnostics, we also report the average matched-node mask and label terms separately:

$$MQ = \frac{1}{|TP_{\text{node}}|} \sum_{(\hat{v}, v) \in TP_{\text{node}}} \text{IoU}(\hat{v}, v), \quad LQ_m = \frac{1}{|TP_{\text{node}}|} \sum_{(\hat{v}, v) \in TP_{\text{node}}} \text{Sim}_m(\hat{\ell}_{\hat{v}}, \ell_v). \quad (4)$$

4.3 Branch Quality and Open Tree Quality

Tree quality evaluates whether recovered tree preserve the visual organization of the reference tree. Exact edge matching can be overly strict for open tree decomposition because a prediction may insert or skip an intermediate node while preserving the larger visual ancestor. We therefore compare nearest matched common parents on the matched mask-node skeleton.

Let r_G and r_P denote the artificial roots of the reference tree G and the predicted tree P , respectively. We form a TP-matched skeleton for each tree by keeping only the true-positive matched nodes and the artificial root. For parent assignment, we climb the original semantic-label tree one level at a time and attach the mask-node to the highest-IoU mask under the first ancestor label with positive overlap.

Let G^{TP} and P^{TP} denote the resulting reference and prediction skeletons.

for matched masks m_i and m_j , we define their nearest matched common parents as

$$p_G(m_i, m_j) = \text{LCA}_{G^{TP}}(v_i, v_j), \quad p_P(m_i, m_j) = \text{LCA}_{P^{TP}}(\hat{v}_i, \hat{v}_j). \quad (5)$$

A pair is branch-consistent when the reference-side nearest matched common parent maps to the prediction-side nearest matched common parent:

$$C(m_i, m_j) = \mathbf{1}[p_G(m_i, m_j) = p_P(m_i, m_j)]. \quad (6)$$

Table 5: Controlled GT degradation audit with BERT label similarity.

GT variant	Main corruption	HPQ↑	OTQ↑	TQ↑	meanNQ↑	MQ↑	LQ↑
GT	-	1	1	1	1	1	1
mask erosion 50%	shrink masks	0.323	0.352	0.706	0.498	0.508	0.983
mask dilation 50%	expand masks	0.670	0.640	0.979	0.653	0.668	0.978
parent rewiring 50%	change parents	0.203	0.778	0.778	1.000	1.000	1.000
internal-semantic-node missing 50%	remove internal nodes	0.897	0.915	0.915	1.000	1.000	1.000
leaf-semantic-node missing 50%	remove leaf nodes	0.477	0.785	0.785	1.000	1.000	1.000
random-semantic-node missing 50%	remove random nodes	0.491	0.652	0.652	1.000	1.000	1.000

Let

$$\mathcal{P}_{TP} = \{\{m_i, m_j\} \mid m_i, m_j \in TP_{\text{node}}, i < j\} \quad (7)$$

be all unordered pairs of true-positive mask-node matches. The branch-pair accuracy is

$$BQ = \begin{cases} 1, & |\mathcal{P}_{TP}| = 0, \\ \frac{1}{|\mathcal{P}_{TP}|} \sum_{\{m_i, m_j\} \in \mathcal{P}_{TP}} C(m_i, m_j), & |\mathcal{P}_{TP}| > 0. \end{cases} \quad (8)$$

Tree quality applies a PQ-style recovery penalty to the branch-pair accuracy:

$$TQ = BQ \cdot \frac{|TP_{\text{node}}|}{|TP_{\text{node}}| + \frac{1}{2}|FP_{\text{node}}| + \frac{1}{2}|FN_{\text{node}}|}. \quad (9)$$

Thus, BQ measures whether recovered mask-nodes preserve visual organization, while the denominator penalizes missing and spurious mask-nodes.

Finally, Open Tree Quality combines tree quality with matched-node quality:

$$OTQ_m = TQ \cdot \text{meanNQ}_m. \quad (10)$$

This expanded form shows that OTQ extends the PQ-style evaluation benchmark by incorporating open-label-aware matching, matched-node quality meanNQ_m , and tree-structure similarity TQ.

4.4 Metric Test with Controlled Degradations

We first tested OTQ using controlled degradations of the GT reference trees on the same 1K-image human-validation subset described in Section 3.3. This experiment verifies whether the evaluator responds to the intended failure modes. Starting from the GT tree, we perturb masks, remove nodes, or rewire parents while preserving the other evidence as much as possible (more results in Appendix E.1).

Table 5 reports representative GT degradations. Mask erosion and dilation reduce matched-node quality, as reflected by lower meanNQ and MQ. Parent rewiring keeps masks and labels unchanged, so meanNQ, MQ, and LQ remain near one, while TQ drops because the visual parent structure is corrupted. Node or label-node removal mainly reduces TQ, since the remaining matched nodes still have high local mask and label quality.

4.5 Benchmark Trees

We next evaluated non-identical trees against the released references. This comparison includes flat projections from existing coco-based datasets and recursive SAM 3-based trees. For the recursive baseline, we crop each semantic bounding box and recursively call SAM 3 inside the crop. We further evaluate corrupted recursive variants to check whether the benchmark exposes missing masks, degraded masks, and wrong parent assignments.

Table 6 shows benchmark results with recursively generated SAM 3 outputs and other datasets. HPQ provides a useful hierarchy-oriented reference score, while OTQ further decomposes each result into tree quality and matched-node quality. Flat projections retain nonzero local mask and label quality, but their low TQ shows that they lack image-specific tree relations. For recursive variants, OTQ exposes whether degradation comes from mask quality, missing nodes, or rewired parent structure.

Table 6: Benchmark tree comparison with BERT label similarity. Note that COCO-Stuff does not provide instance masks

Tree source	Images	HPQ \uparrow	OTQ \uparrow	TQ \uparrow	meanNQ \uparrow	MQ \uparrow	LQ \uparrow
COCO-17 flat projection	20.9K	0.020	0.098	0.125	0.781	0.829	0.929
COCONut flat projection	4.9K	0.021	0.107	0.132	0.810	0.857	0.932
COCO-ReM flat projection	20.9K	0.022	0.119	0.140	0.849	0.904	0.928
LVIS flat projection	21.1K	0.024	0.115	0.146	0.764	0.841	0.882
Recursive_output_tree	1K	0.349	0.587	0.655	0.895	0.901	0.994
Recursive + mask erosion 50%	1K	0.075	0.208	0.398	0.521	0.537	0.969
Recursive + mask dilation 50%	1K	0.219	0.397	0.620	0.640	0.653	0.982
Recursive + parent rewiring 50%	1K	0.071	0.469	0.522	0.895	0.901	0.994
Recursive + internal-semantic-node missing 50%	1K	0.339	0.525	0.592	0.885	0.893	0.991
Recursive + leaf-semantic-node missing 50%	1K	0.165	0.444	0.490	0.905	0.910	0.993
Recursive + random-semantic-node missing 50%	1K	0.191	0.356	0.403	0.881	0.891	0.987

5 Discussion and Limitations

Reference multiplicity. A fundamental challenge in open tree decomposition is the existence of multiple valid solutions. Because hierarchical parsing is an unconstrained task, a single scene can be logically decomposed in several ways, leading to natural variations in node grouping, intermediate depth, and terminal leaf selection. Therefore, we established COCOTREE under strict human validation and consensus to provide a singular, high-fidelity reference structure.

Open-vocabulary evaluation. Open labels make the benchmark more flexible than fixed-category part datasets, but they also make label evaluation less direct. The label term in OTQ relies on a label-similarity protocol, which may introduce errors or biases for synonyms, rare words, or parent-dependent meanings. Although we strictly mitigate this lexical ambiguity by evaluating text labels in conjunction with their matched geometric masks and topological tree positions, the inherent fuzziness of automated open-text evaluation remains a structural source of measurement uncertainty.

Automated annotation errors. Fully automated recursive pipelines inevitably introduce structural and geometric noise. Specifically, the generation process can occasionally miss small child nodes, produce noisy masks, or duplicate redundant instances. These issues are especially prevalent in highly localized, deep-tier regions of the hierarchy. Our comprehensive analysis also revealed these limitations present in COCOTREE, thus opening new future research directions for robust, self-verifying automated annotation frameworks.

6 Conclusion

We introduced COCOTREE, a COCO-based dataset and benchmark for *open tree decomposition*. COCOTREE represents each image as an open-vocabulary tree of visible instances, where each node is grounded by a single instance mask and a local semantic label. This moves segmentation beyond flat region prediction and fixed object-part templates toward image-specific structural understanding. We constructed COCOTREE with a fully automated recursive annotation pipeline that uses LVLMs for parent-conditioned child proposal and the vision foundation model (SAM3) for mask grounding. The dataset contains over 21K images, 1.8M instance nodes, 85.7 masks per image, and more than 3.5K open-vocabulary labels. Human validation showed that the generated references are reliable across label, mask, and structural axes. We also proposed Open Tree Quality (OTQ), a PQ-style metric that jointly evaluates node recovery, mask quality, label quality, and visual parent consistency. Together, COCOTREE and OTQ define a benchmark for models that must recover not only visible regions but also their compositional organization. We believe this setting opens a path toward segmentation systems that better support fine-grained reasoning, interaction, and embodied visual understanding.

Broader impacts. As with any automatically constructed visual dataset, COCOTREE should not be treated as a complete or error-free description of visual structure. Models trained on it may inherit annotation errors, dataset biases, or failures on small and ambiguous regions.

References

- [1] Holger Caesar, Jasper Uijlings, and Vittorio Ferrari. Coco-stuff: Thing and stuff classes in context. In *Proceedings of the IEEE Conference on Computer Vision and Pattern Recognition (CVPR)*, June 2018.
- [2] Nicolas Carion, Laura Gustafson, Yuan-Ting Hu, Shoubhik Debnath, Ronghang Hu, Didac Suris, Chaitanya Ryali, Kalyan Vasudev Alwala, Haitham Khedr, Andrew Huang, Jie Lei, Tengyu Ma, Baishan Guo, Arpit Kalla, Markus Marks, Joseph Greer, Meng Wang, Peize Sun, Roman Rädle, Triantafyllos Afouras, Effrosyni Mavroudi, Katherine Xu, Tsung-Han Wu, Yu Zhou, Liliane Momeni, Rishi Hazra, Shuangrui Ding, Sagar Vaze, Francois Porcher, Feng Li, Siyuan Li, Aishwarya Kamath, Ho Kei Cheng, Piotr Dollár, Nikhila Ravi, Kate Saenko, Pengchuan Zhang, and Christoph Feichtenhofer. SAM 3: Segment anything with concepts. *arXiv preprint arXiv:2511.16719*, 2026.
- [3] Xianjie Chen, Roozbeh Mottaghi, Xiaobai Liu, Sanja Fidler, Raquel Urtasun, and Alan Yuille. Detect what you can: Detecting and representing objects using holistic models and body parts. In *Proceedings of the IEEE Conference on Computer Vision and Pattern Recognition*, pages 1971–1978, 2014.
- [4] Yi-Chia Chen, Wei-Hua Li, Cheng Sun, Yu-Chiang Frank Wang, and Chu-Song Chen. SAM4MLLM: Enhance multi-modal large language model for referring expression segmentation. *arXiv preprint arXiv:2409.10542*, 2024.
- [5] Daan de Geus, Panagiotis Meletis, Chenyang Lu, Xiaoxiao Wen, and Gijs Dubbelman. Part-aware panoptic segmentation. In *Proceedings of the IEEE/CVF Conference on Computer Vision and Pattern Recognition*, pages 5481–5490, 2021.
- [6] Xueqing Deng, Qihang Yu, Peng Wang, Xiaohui Shen, and Liang-Chieh Chen. COCONut: Modernizing coco segmentation. In *Proceedings of the IEEE/CVF Conference on Computer Vision and Pattern Recognition*, pages 21863–21873, 2024.
- [7] Jacob Devlin, Ming-Wei Chang, Kenton Lee, and Kristina Toutanova. BERT: Pre-training of deep bidirectional transformers for language understanding. In *Proceedings of the 2019 Conference of the North American Chapter of the Association for Computational Linguistics: Human Language Technologies*, pages 4171–4186, 2019.
- [8] Agrim Gupta, Piotr Dollár, and Ross Girshick. LVIS: A dataset for large vocabulary instance segmentation. In *Proceedings of the IEEE/CVF Conference on Computer Vision and Pattern Recognition*, pages 5356–5364, 2019.
- [9] Ju He, Shuo Yang, Shaokang Yang, Adam Kortylewski, Xiaoding Yuan, Jie-Neng Chen, Shuai Liu, Cheng Yang, Qihang Yu, and Alan Yuille. PartImageNet: A large, high-quality dataset of parts. In *Computer Vision – ECCV 2022*, pages 128–145. Springer, 2022.
- [10] Kaiming He, Georgia Gkioxari, Piotr Dollár, and Ross Girshick. Mask r-cnn. In *Proceedings of the IEEE International Conference on Computer Vision*, pages 2961–2969, 2017.
- [11] Alexander Kirillov, Kaiming He, Ross Girshick, Carsten Rother, and Piotr Dollár. Panoptic segmentation. In *Proceedings of the IEEE/CVF Conference on Computer Vision and Pattern Recognition*, pages 9404–9413, 2019.
- [12] Alexander Kirillov, Eric Mintun, Nikhila Ravi, Hanzi Mao, Chloe Rolland, Laura Gustafson, Tete Xiao, Spencer Whitehead, Alexander C. Berg, Wan-Yen Lo, Piotr Dollár, and Ross Girshick. Segment anything. In *Proceedings of the IEEE/CVF International Conference on Computer Vision*, pages 4015–4026, 2023.
- [13] Xin Lai, Zhuotao Tian, Yukang Chen, Yanwei Li, Yuhui Yuan, Shu Liu, and Jiaya Jia. LISA: Reasoning segmentation via large language model. In *Proceedings of the IEEE/CVF Conference on Computer Vision and Pattern Recognition*, 2024.
- [14] Feng Li, Hao Zhang, Peize Sun, Xueyan Zou, Shilong Liu, Jianwei Yang, Chunyuan Li, Lei Zhang, and Jianfeng Gao. Semantic-SAM: Segment and recognize anything at any granularity. *arXiv preprint arXiv:2307.04767*, 2023.

- [15] Liulei Li, Tianfei Zhou, Wenguan Wang, Jianwu Li, and Yi Yang. Deep hierarchical semantic segmentation. In *Proceedings of the IEEE/CVF Conference on Computer Vision and Pattern Recognition*, pages 1236–1247, 2022.
- [16] Xiangtai Li, Shilin Xu, Jinheng Yang, Guangliang Cheng, Yunhai Tong, and Dacheng Tao. Panoptic-partformer: Learning a unified model for panoptic part segmentation. In *Computer Vision – ECCV 2022*. Springer, 2022.
- [17] Tsung-Yi Lin, Michael Maire, Serge Belongie, James Hays, Pietro Perona, Deva Ramanan, Piotr Dollár, and C. Lawrence Zitnick. Microsoft coco: Common objects in context. In *Computer Vision – ECCV 2014*, pages 740–755. Springer, 2014.
- [18] Haotian Liu, Chunyuan Li, Qingyang Wu, and Yong Jae Lee. Visual instruction tuning, 2023. URL <https://arxiv.org/abs/2304.08485>.
- [19] Jonathan Long, Evan Shelhamer, and Trevor Darrell. Fully convolutional networks for semantic segmentation. In *Proceedings of the IEEE Conference on Computer Vision and Pattern Recognition*, pages 3431–3440, 2015.
- [20] John P. McCrae, Alexandre Rademaker, Ewa Rudnicka, and Francis Bond. English WordNet 2020: Improving and extending a WordNet for english using an open-source methodology. In *Proceedings of the LREC 2020 Workshop on Multimodal Wordnets*, pages 14–19, Marseille, France, 2020. European Language Resources Association.
- [21] Panagiotis Meletis, Xiaoxiao Wen, Chenyang Lu, Daan de Geus, and Gijs Dubbelman. Cityscapes-panoptic-parts and PASCAL-panoptic-parts datasets for scene understanding. *arXiv preprint arXiv:2004.07944*, 2020.
- [22] George A. Miller. WordNet: A lexical database for english. *Communications of the ACM*, 38(11):39–41, 1995.
- [23] Josh Myers-Dean, Brian Price, Yifei Fan, and Danna Gurari. Hierarchical semantic segmentation with autoregressive language modeling. In *Proceedings of the IEEE/CVF Conference on Computer Vision and Pattern Recognition Workshops*, pages 4120–4130, 2025.
- [24] Josh Myers-Dean, Jarek Reynolds, Brian Price, Yifei Fan, and Danna Gurari. Spin: Hierarchical segmentation with subpart granularity in natural images. In Aleš Leonardis, Elisa Ricci, Stefan Roth, Olga Russakovsky, Torsten Sattler, and Gül Varol, editors, *Computer Vision – ECCV 2024*, pages 275–292, Cham, 2025. Springer Nature Switzerland. ISBN 978-3-031-72691-0.
- [25] Alec Radford, Jong Wook Kim, Chris Hallacy, Aditya Ramesh, Gabriel Goh, Sandhini Agarwal, Girish Sastry, Amanda Askell, Pamela Mishkin, Jack Clark, Gretchen Krueger, and Ilya Sutskever. Learning transferable visual models from natural language supervision. In *Proceedings of the 38th International Conference on Machine Learning*, volume 139 of *Proceedings of Machine Learning Research*, pages 8748–8763. PMLR, 2021.
- [26] Vignesh Ramanathan, Anmol Kalia, Vladan Petrovic, Yi Wen, Baixue Zheng, Baishan Guo, Rui Wang, Aaron Marquez, Rama Kovvuri, Abhishek Kadian, Amir Mousavi, Yiwen Song, Abhimanyu Dubey, and Dhruv Mahajan. Paco: Parts and attributes of common objects. In *Proceedings of the IEEE/CVF Conference on Computer Vision and Pattern Recognition*, pages 7141–7151, 2023.
- [27] Hanoona Rasheed, Muhammad Maaz, Sahal Shaji, Abdelrahman Shaker, Salman Khan, Hisham Cholakkal, Rao M. Anwer, Eric Xing, Ming-Hsuan Yang, and Fahad S. Khan. Glamm: Pixel grounding large multimodal model. In *Proceedings of the IEEE/CVF Conference on Computer Vision and Pattern Recognition (CVPR)*, pages 13009–13018, June 2024.
- [28] Nils Reimers and Iryna Gurevych. Sentence-BERT: Sentence embeddings using siamese BERT-networks. In *Proceedings of the 2019 Conference on Empirical Methods in Natural Language Processing and the 9th International Joint Conference on Natural Language Processing*, pages 3982–3992. Association for Computational Linguistics, 2019.

- [29] Zhongwei Ren, Zhicheng Huang, Yunchao Wei, Yao Zhao, Dongmei Fu, Jiashi Feng, and Xiaojie Jin. PixelLM: Pixel reasoning with large multimodal model. In *Proceedings of the IEEE/CVF Conference on Computer Vision and Pattern Recognition*, 2024.
- [30] Shweta Singh, Aayan Yadav, Jitesh Jain, Humphrey Shi, Justin Johnson, and Karan Desai. Benchmarking object detectors with coco: A new path forward. In *European Conference on Computer Vision (ECCV)*. Springer, 2024.
- [31] Chufeng Tang, Lingxi Xie, Xiaopeng Zhang, Xiaolin Hu, and Qi Tian. Visual recognition by request. In *Proceedings of the IEEE/CVF Conference on Computer Vision and Pattern Recognition*, pages 15265–15274, 2023.
- [32] Junchi Wang and Lei Ke. Llm-seg: Bridging image segmentation and large language model reasoning, 2024. URL <https://arxiv.org/abs/2404.08767>.
- [33] Xudong Wang, Shufan Li, Konstantinos Kallidromitis, Yusuke Kato, Kazuki Kozuka, and Trevor Darrell. HIPIE: Hierarchical open-vocabulary universal image segmentation. In *Advances in Neural Information Processing Systems*, 2023.
- [34] XuDong Wang, Shaolun Zhang, Shufan Li, Konstantinos Kallidromitis, Kehan Li, Yusuke Kato, Kazuki Kozuka, and Trevor Darrell. SegLLM: Multi-round reasoning segmentation. *arXiv preprint arXiv:2410.18923*, 2024.
- [35] Xu Zhang, Junyao Ge, Yang Zheng, Kaitai Guo, and Jimin Liang. Bridging semantics and geometry: A decoupled LVLN-SAM framework for reasoning segmentation in optical remote sensing. *arXiv preprint arXiv:2512.19302*, 2025.
- [36] Bolei Zhou, Hang Zhao, Xavier Puig, Tete Xiao, Sanja Fidler, Adela Barriuso, and Antonio Torralba. Semantic understanding of scenes through the ade20k dataset. *International Journal of Computer Vision*, 127(3):302–321, 2019.

A Prompt Details

This appendix summarizes the prompts used by the LVLM planner in our construction pipeline. The prompts are designed to produce visible, recognizable, separable, and structurally meaningful child labels while avoiding hidden or merely expected parts.

A.1 System Prompt

Objective. The system prompt asks the planner to produce a rich hierarchy of visible structure. It encourages decomposition whenever clear and visually supported subparts exist. It also prefers continuing decomposition over stopping early.

Evidence policy.

- Use only visible evidence from the image or masked crop.
- Do not infer hidden, occluded, or merely expected parts.
- Propose a candidate only when it is visually supported and reasonably separable.
- Prefer decompositions that reveal more meaningful visible structure.
- If an intermediate part is unclear but a finer part is clearly visible, propose the finer part directly.

Hierarchy policy.

- Continue decomposition whenever another meaningful visible level can be exposed.
- Require each child to be a meaningful subpart of its parent.
- Prefer structural parts, functional parts, attached components, and clearly bounded visible regions.
- Prefer larger structural parts when they are clear, while still allowing smaller visible parts.
- Prefer intermediate levels when they are visible and separable, but do not force them when they are unclear.
- Avoid outputting a parent like concept and its likely internal subpart in the same step.
- Stop only when no further clear, recognizable, visually separable, and structurally meaningful subpart can be proposed.

Rejection policy.

- Do not propose materials, textures, colors, patterns, lighting effects, reflections, shadows, or abstract concepts.
- Do not propose labels that are too vague or that merely restate the parent or an ancestor.
- Do not invent nonvisible parts.
- Do not output duplicates, near synonyms, or overlapping alternatives for the same region.
- Do not propose boundary only regions such as rims, borders, outlines, edges, or outer rings unless they are distinct physical components.
- Do not split an object into an outer band and inner area when the split follows only silhouette, perimeter, or graphic layout.

Label policy.

- Use singular concrete nouns.
- Prefer common everyday words.
- Prefer one word and use two words only for common compound nouns.
- Avoid adjectives, attributes, colors, materials, positions, lighting terms, and abstract words.
- Avoid punctuation, quotes, and duplicate labels.

- If labels overlap strongly, keep one label and prefer the more common term unless the finer term reveals a meaningful decomposition level.
- Avoid technical, scientific, anatomical, or highly specialized terms.

A.2 Initial Root Discovery Prompt

The initial discovery prompt proposes root level anchors that maximize visible coverage and support later decomposition. It is intentionally biased toward larger visible units because internal parts can be discovered in later parent conditioned steps.

- Propose root level units only.
- Prefer whole objects and major scene regions that can act as strong anchors.
- Include dominant scene regions such as sky, ground, water, road, mountain, wall, floor, and ceiling when clearly visible.
- Include distinct whole objects such as person, car, building, animal, furniture, plant, container, tool, and appliance.
- Maximize coverage of major visible structure.
- Prefer candidates that enable rich later decomposition.
- Do not propose internal parts when a larger visible object can serve as the root anchor.
- If one candidate is likely a part of another visible candidate, propose only the larger candidate at this step.
- Avoid tiny fragments, textures, materials, coverings, duplicates, synonyms, positional variants, and overly abstract scene labels.
- Propose enough roots for strong coverage and later decomposition, typically between four and twenty four candidates.

A.3 Local Decomposition Prompt

The local decomposition prompt expands multiple accepted parent nodes in a batch. For each parent, the LVLMM receives the masked crop and current path, then proposes child labels using only the masked crop as visual evidence.

- Process each parent independently.
- Use the path and label only for filtering and context, not for inventing unseen parts.
- Do not stop if clear subparts exist.
- Propose as many meaningful visible subparts as can be supported, up to the configured maximum number of children.
- Prefer structural parts, functional parts, attached components, and clearly bounded visible regions.
- Prefer intermediate levels when they are clearly supported and separable.
- If an intermediate level is unclear but a finer part is visible and commonly recognized, propose the finer part directly.
- Keep children at a similar structural level when possible.
- Allow attached accessories, appendages, and externally visible components as direct children.
- Avoid materials, textures, colors, patterns, coverings, and surface layers.
- Return an empty child list when no clear, recognizable, visually separable, and meaningful subpart can be proposed.

A.4 Output Contract

The prompt requires structured tool output so that proposals can be parsed and audited automatically. For initial discovery, the output is a list of root text prompts. For local decomposition, the output includes every parent identifier exactly once and assigns each parent either a list of child prompts or an empty list. The planner is instructed to return only the tool call and no free form explanation.

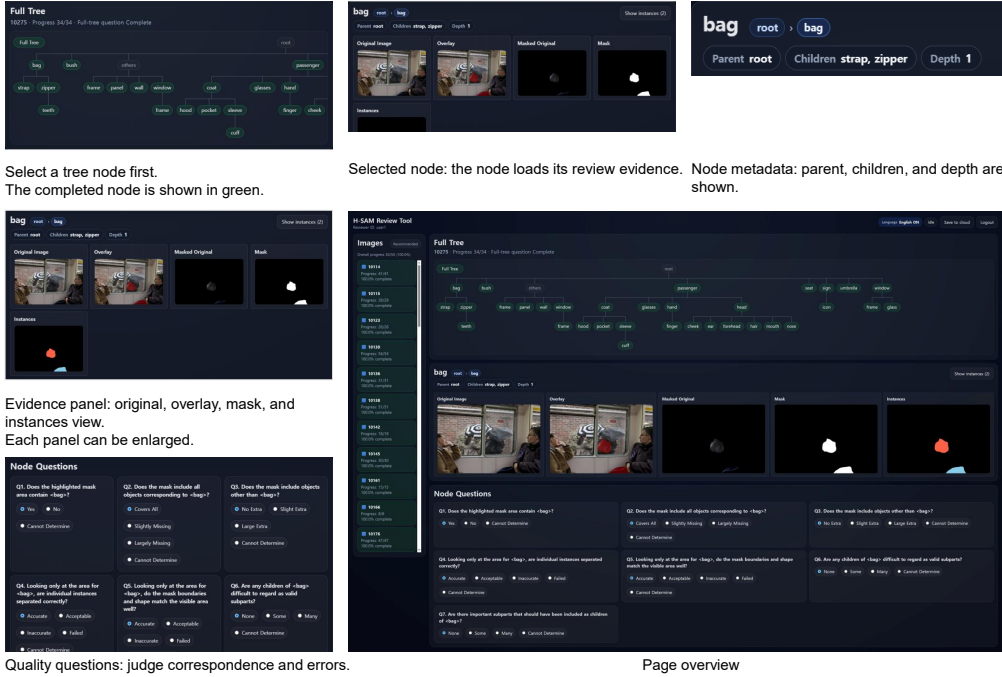


Figure 3: Review website interface used for human evaluation. Reviewers used this interface to inspect the image, annotation hierarchy, masks, and evaluation questions.

B Review Website

Figure 3 shows the website interface used by reviewers to evaluate the annotations.

B.1 Human Validation Questions

The reviewers evaluated each sampled annotation through semantic-node-level and tree-level questions. For each node, the interface showed the original image, the parent context, the highlighted target mask, the local node label, and the current tree path. The placeholder <Label> was replaced with the local label of the evaluated node.

All reviewers first answered the five mask- and label-related questions Q1–Q5. Then, the question set depended on whether the evaluated node was a leaf. For non-leaf nodes, reviewers answered Q6–Q7 to assess whether the children were valid and sufficiently complete. For leaf nodes, reviewers answered Q8 to assess whether stopping the decomposition at that node was appropriate. After all semantic-node-level questions for an image were completed, the reviewers answered two full-tree questions, T1 and T2, to assess global decomposition quality and whether meaningful regions remained unannotated.

C Dataset distribution

Figure 4 shows the label distribution of all valid nodes in COCOTREE. Only images that passed the strict integrity check were included. Nodes whose terminal label was others were excluded before computing the distribution. Each rectangle represents one label, and its area is proportional to the fraction of counted nodes assigned to that label.

Figure 5 summarizes the per-image complexity of COCOTREE. The x-axis groups images by the number of masks per image in bins of 25, while the y-axis groups images by the number of unique labels per image in bins of 10. Each cell reports the number of images that fall into the corresponding mask-label range.

Table 7: Human validation questions. Q1–Q5 were answered for every evaluated node. Q6–Q7 were answered only for non-leaf semantic-nodes, while Q8 was answered only for leaf semantic-nodes. After all semantic-node-level questions were completed for an image, reviewers answered the full-tree questions T1–T2.

ID	Scope	Axis	Question shown to reviewers	Response options
Q1	All nodes	Label-mask match	Does the highlighted mask area contain <Label>?	Yes; No; Cannot determine
Q2	All nodes	Target coverage	Does the mask include all objects corresponding to <Label>?	Covers all; Slightly missing; Largely missing; Cannot determine
Q3	All nodes	Extra region	Does the mask include objects other than <Label>?	No extra; Slight extra; Large extra; Cannot determine
Q4	All nodes	Instance separation	Looking only at the area for <Label>, are individual instances separated correctly?	Accurate; Acceptable; Inaccurate; Failed; Cannot determine
Q5	All nodes	Boundary quality	Looking only at the area for <Label>, do the mask boundaries and shape match the visible area well?	Accurate; Acceptable; Inaccurate; Failed; Cannot determine
Q6	Non-leaf only	Child validity	Are any children of <Label> difficult to regard as valid subparts?	None; Some; Many; Cannot determine
Q7	Non-leaf only	Missing children	Are there important subparts that should have been included as children of <Label>?	None; Some; Many; Cannot determine
Q8	Leaf only	Leaf stopping	Is it appropriate not to subdivide <Label> any further here?	Yes; No; Cannot determine
T1	Full tree	Tree consistency	Does the full tree appropriately decompose the image?	Correct; Mostly correct; Partly correct; Incorrect; Cannot determine
T2	Full tree	Remaining area	Are there meaningful elements in the remaining area?	None; Some; Many; Cannot determine

D Annotation Center Distribution

Figure 6 shows the spatial distribution of annotation centers in the reviewed samples. This visualization provides an overview of where annotated regions tend to appear in the image plane and helps summarize the spatial coverage of the evaluation set.

E Additional OTQ Evaluation Results

This appendix provides the full component-level results for the controlled degradation and baseline comparison experiments used in Sec. 4.4 and Sec. 4.5. All OTQ values use BERT-based label similarity. We report HPQ as a prior hierarchy-oriented reference score and decompose OTQ into tree quality TQ, matched-node quality meanNQ, mask quality MQ, and label quality LQ. Here, TQ captures node recovery and parent-structure consistency, while meanNQ captures the average quality of true-positive matched nodes.

E.1 Controlled GT Degradations

This appendix provides the full component-level results for controlled corruptions. Table 8 reports controlled corruptions applied to the GT reference trees. Each variant changes one aspect of the

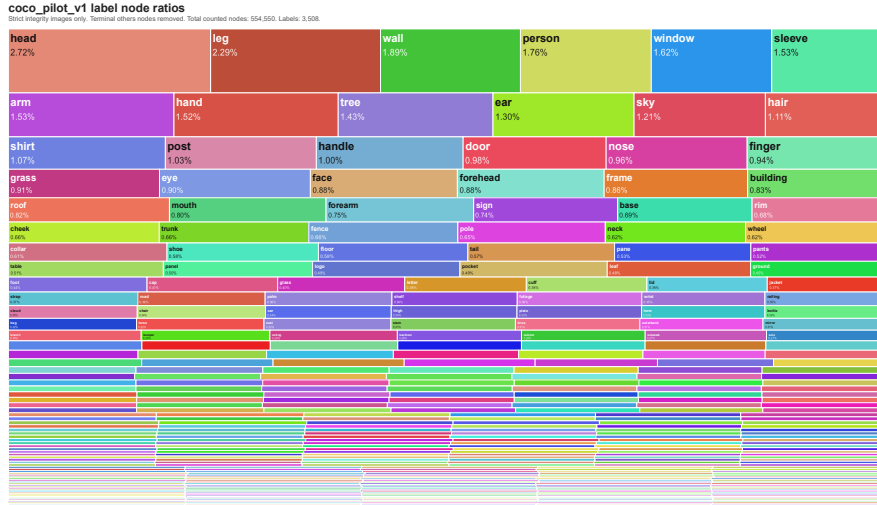


Figure 4: Label distribution treemap for COCOTREE.

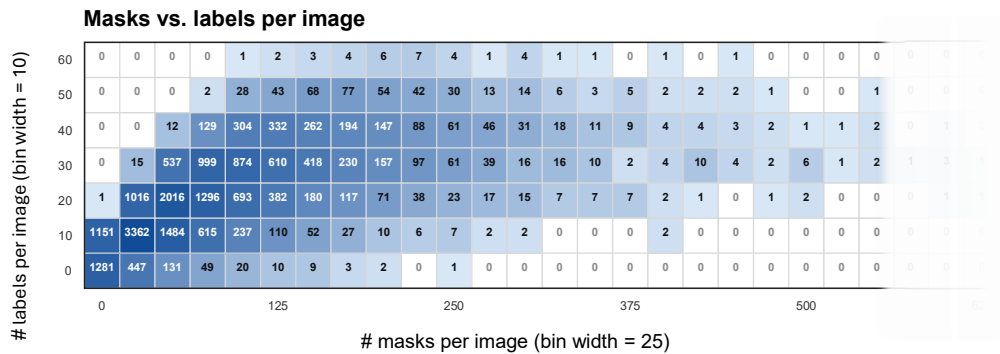


Figure 5: Joint distribution of masks and labels per image in COCOTREE. The horizontal axis shows the number of masks per image using 25-mask bins, and the vertical axis shows the number of unique labels per image using 10-label bins.

reference while preserving the others as much as possible. Mask erosion and dilation perturb mask geometry, parent rewiring changes the tree structure while keeping masks and labels unchanged, and label-missing variants remove semantic label units from different parts of the tree. The keep ratio controls the remaining portion of the original evidence, with lower ratios corresponding to stronger corruption.

The results show that the OTQ components respond to the intended failure modes. Mask erosion and dilation reduce MQ and meanNQ because the matched masks become less accurate. Parent rewiring keeps MQ, LQ, and meanNQ at one, but lowers TQ, confirming that the structural error is isolated in the tree-quality term. For internal semantic-label missing, HPQ and OTQ drops while meanNQ remains high. OTQ reflects the loss through TQ.

E.2 Recursive SAM 3 Corruption Results

Table 9 reports the same corruption protocol on recursive SAM 3-based trees.

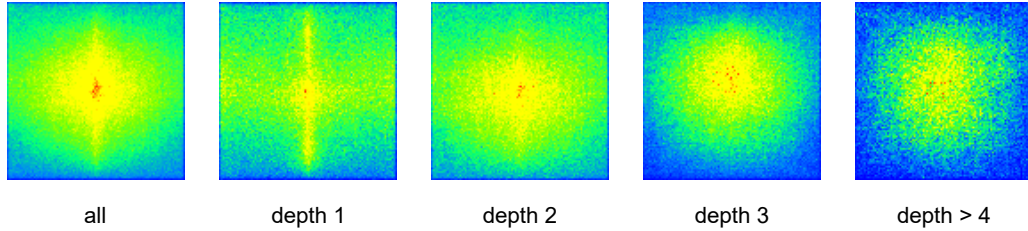


Figure 6: Spatial distribution of annotation centers in the reviewed samples. The plot summarizes where annotated regions are located across the image plane, providing a compact view of the evaluation set’s spatial coverage.

Table 8: Controlled GT degradation results.

Variant	Keep ratio	HPQ \uparrow	OTQ \uparrow	TQ \uparrow	meanNQ \uparrow	MQ \uparrow	LQ \uparrow
gt_oracle_tree	-	1	1	1	1	1	1
gt_mask_erosion	75	0.750	0.731	0.990	0.738	0.750	0.984
	50	0.323	0.352	0.706	0.498	0.508	0.983
	30	0.000	0.004	0.009	0.195	0.233	0.343
	15	0.000	0.001	0.002	0.058	0.075	0.100
gt_mask_dilation	75	0.801	0.780	0.990	0.788	0.800	0.984
	50	0.670	0.640	0.979	0.653	0.668	0.978
	30	0.594	0.556	0.963	0.578	0.592	0.977
	15	0.547	0.503	0.943	0.533	0.547	0.977
gt_parent_rewire	75	0.463	0.872	0.872	1.000	1.000	1.000
	50	0.203	0.778	0.778	1.000	1.000	1.000
	30	0.100	0.729	0.729	1.000	1.000	1.000
	15	0.045	0.692	0.692	1.000	1.000	1.000
gt_internal_label_missing	75	0.951	0.964	0.965	1.000	1.000	1.000
	50	0.897	0.915	0.915	1.000	1.000	1.000
	30	0.863	0.873	0.874	1.000	1.000	1.000
	15	0.842	0.842	0.842	1.000	1.000	1.000
gt_leaf_label_missing	75	0.747	0.899	0.899	1.000	1.000	1.000
	50	0.477	0.785	0.785	1.000	1.000	1.000
	30	0.268	0.673	0.673	1.000	1.000	1.000
	15	0.128	0.571	0.571	1.000	1.000	1.000
gt_random_label_missing	75	0.712	0.853	0.854	1.000	1.000	1.000
	50	0.491	0.652	0.652	1.000	1.000	1.000
	30	0.303	0.451	0.451	1.000	1.000	1.000
	15	0.146	0.263	0.263	0.996	0.996	0.996

The similar degradation trends between OTQ and HPQ suggest that OTQ preserves the hierarchy-sensitive behavior of HPQ while extending it to open-label settings through explicit label-quality evaluation.

E.3 Label similarity method

Table 10 reports flat projection results under different label-similarity protocols. Because TQ depends on node recovery and parent-structure consistency, it remains unchanged across label-similarity methods. In contrast, LQ, meanNQ, and OTQ vary with the label protocol. Several label-similarity

Table 9: Corrupted recursive SAM 3-based tree results.

Variant	Keep ratio	HPQ \uparrow	OTQ \uparrow	TQ \uparrow	meanNQ \uparrow	MQ \uparrow	LQ \uparrow
recursive_output_tree	-	0.349	0.587	0.655	0.895	0.901	0.994
recursive_mask_erosion	75	0.247	0.469	0.644	0.727	0.740	0.982
	50	0.075	0.208	0.398	0.521	0.537	0.969
	30	0.000	0.005	0.009	0.185	0.213	0.330
	15	0.000	0.001	0.002	0.036	0.046	0.062
recursive_mask_dilation	75	0.279	0.481	0.640	0.752	0.763	0.985
	50	0.219	0.397	0.620	0.640	0.653	0.982
	30	0.181	0.336	0.585	0.575	0.587	0.980
	15	0.154	0.281	0.523	0.537	0.549	0.979
recursive_parent_rewire	75	0.157	0.528	0.589	0.895	0.901	0.994
	50	0.071	0.469	0.522	0.895	0.901	0.994
	30	0.031	0.431	0.481	0.895	0.901	0.994
	15	0.012	0.405	0.452	0.895	0.901	0.994
recursive internal-semantic-node missing	75	0.343	0.560	0.628	0.891	0.898	0.992
	50	0.339	0.525	0.592	0.885	0.893	0.991
	30	0.333	0.497	0.561	0.884	0.893	0.990
	15	0.331	0.475	0.540	0.879	0.888	0.989
recursive leaf-semantic-node missing	75	0.250	0.523	0.580	0.901	0.907	0.994
	50	0.165	0.444	0.490	0.905	0.910	0.993
	30	0.094	0.363	0.398	0.907	0.913	0.989
	15	0.049	0.309	0.339	0.903	0.909	0.984
recursive random-semantic-node missing	75	0.267	0.484	0.541	0.893	0.900	0.993
	50	0.191	0.356	0.403	0.881	0.891	0.987
	30	0.111	0.246	0.272	0.900	0.908	0.989
	15	0.059	0.130	0.150	0.842	0.854	0.962

protocols are supported, while relative comparisons remain meaningful as long as the same protocol is used across datasets or methods. The LQ1 setting assigns $LQ = 1$ to every true-positive match, providing a label-agnostic upper-bound view of mask and tree quality. The strict setting assigns a positive label score only for exact label matches, providing a conservative evaluation of open-label agreement. Overall, the results show that flat resources can retain nonzero mask quality, but their lack of image-specific tree structure keeps TQ low.

Table 10: Flat projection results under different label-similarity protocols. TQ is unchanged across label-similarity methods because it depends only on node recovery and tree structure, while meanNQ and OTQ vary with the label-quality protocol.

Variant	Label sim.	OTQ \uparrow	TQ \uparrow	meanNQ \uparrow	MQ \uparrow	LQ \uparrow
COCO	BERT	0.098	0.125	0.781	0.829	0.929
	LQ1	0.104	0.125	0.829	0.829	0.987
	OEWN	0.099	0.125	0.788	0.829	0.936
	Qwen	0.095	0.125	0.761	0.829	0.903
	Strict	0.076	0.125	0.609	0.829	0.721
COCONut	BERT	0.107	0.132	0.810	0.857	0.932
	LQ1	0.113	0.132	0.857	0.857	0.987
	OEWN	0.108	0.132	0.818	0.857	0.940
	Qwen	0.104	0.132	0.791	0.857	0.908
	Strict	0.084	0.132	0.635	0.857	0.727
COCO-ReM	BERT	0.119	0.140	0.849	0.904	0.928
	LQ1	0.127	0.140	0.904	0.904	0.989
	OEWN	0.120	0.140	0.857	0.904	0.936
	Qwen	0.116	0.140	0.825	0.904	0.900
	Strict	0.092	0.140	0.652	0.904	0.707
LVIS	BERT	0.115	0.146	0.764	0.841	0.882
	LQ1	0.126	0.146	0.841	0.841	0.972
	OEWN	0.117	0.146	0.780	0.841	0.899
	Qwen	0.113	0.146	0.748	0.841	0.861
	Strict	0.072	0.146	0.462	0.841	0.529